Phonon dispersion and anomalies in one-layer high-temperature superconductors



2010 J. Phys.: Condens. Matter 22 055404

(http://iopscience.iop.org/0953-8984/22/5/055404)

J. Phys.: Condens. Matter **22** (2010) 149802 (1pp) doi:10.1088/0953-8984/22/14/149802

# Corrigendum

**Phonon dispersion and anomalies in one-layer high-temperature superconductors**

Thomas Bauer and Claus Falter

2010 *J. Phys.: Condens. Matter* **22** 055404

In figure 9(b) of the original manuscript the phonon density of states of $Bi_2Sr_2CuO_6$ has been plotted against the frequency in units of THz and against the energy for convenience also in meV. While the labeling in units of THz is correct, the scale of the labeling in units of meV is wrong. Figure 9(b) with correct labeling is given below.

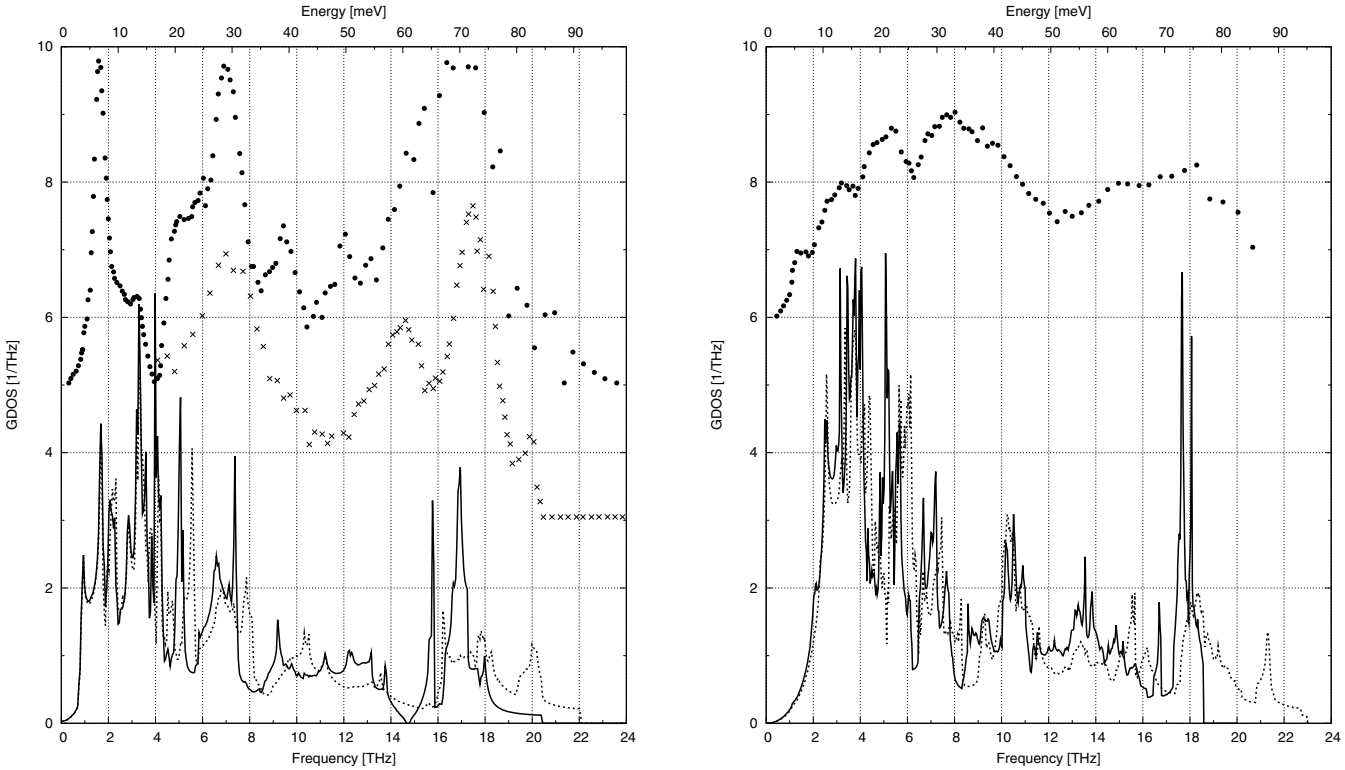


**Figure 9.** Calculated phonon density of states (DOS) for (a) $Hg_2BaCuO_4$ and (b) $Bi_2Sr_2CuO_6$ for model Π-3dim (——). For comparison, the DOS of the RIM is shown as dotted line (· · · · · ·). The symbols × and • in (a) show the experimental data at 30 and 300 K, respectively, the symbols • in (b) represent the experimental data at 300 K. All experimental data are in arbitrary units and shifted for better viewing.

 

IOP PUBLISHING JOURNAL OF PHYSICS: CONDENSED MATTER

J. Phys.: Condens. Matter **22** (2010) 055404 (12pp) doi:10.1088/0953-8984/22/5/055404

# Phonon dispersion and anomalies in one-layer high-temperature superconductors

**Thomas Bauer and Claus Falter**

Institut für Festkörpertheorie, Westfälische Wilhelms-Universität, Wilhelm-Klemm-Straße 10, D-48149 Münster, Germany

E-mail: falter@uni-muenster.de

Received 20 November 2009, in final form 17 December 2009
Published 15 January 2010
Online at stacks.iop.org/JPhysCM/22/055404

**Abstract**

Phonon dynamics, charge response and the phonon density of states are calculated for the high-temperature superconductors $HgBa_2CuO_4$ and $Bi_2Sr_2CuO_6$ within a microscopic model for the electronic density response. The results are compared with previous calculations for $La_2CuO_4$ and $Nd_2CuO_4$. Our main focus is on the phonon anomalies which are connected with the high-frequency oxygen bond-stretching modes (OBSM) found before in our calculations for p-doped $La_2CuO_4$ and n-doped $Nd_2CuO_4$. We investigate the question if the characteristic softening of the OBSM and the related strong coupling to the electrons is also present in $HgBa_2CuO_4$ and $Bi_2Sr_2CuO_6$. In particular, the importance of the contribution of the more delocalized Cu 4s state besides the localized Cu 3d state on the softening is investigated and the different anticrossing behavior due to the presence of several phonon modes with the same symmetry as the OBSM is studied. This makes the identification of the anomalies quite complicated. Furthermore, the influence of electronic polarization processes at ions out of the CuO plane in the ionic layers on the phonon dynamics is calculated. In this context the qualitative type of charge response, i.e. the presence or not of possible metallic charge fluctuations at the Hg or Bi ion, respectively, linked via the apex oxygen to the CuO plane, proves to be very sensitive for certain phonon modes. All the calculations are compared to the experimental results available so far. The latter, however, are rather incomplete for the Hg and Bi compounds.

## 1. Introduction

In the recent literature there is increasing evidence that the electron–phonon interaction (EPI) is significant in cuprate-based high-temperature superconductors (HTSCs) and it is argued that phonons might play an important role for the electron dynamics in the HTSCs; see, e.g., [1–8]. It has been known from experiments for some time that the frequencies of the oxygen bond-stretching modes (OBSM) are strongly renormalized (softened) upon doping in the p-doped cuprates [3, 9–15]. Quite recently the first evidence of an anomalous dispersion of the OBSM has also been reported in a Bi cuprate [16] which, among other things, will be investigated theoretically in this work. Anomalous softening of the OBSM, not existing in the undoped insulating state, has also been observed in the n-doped metallic state of $Nd_2CuO_4$ [17–19]. The phonon dispersion and the charge response in $Nd_2CuO_4$ have been calculated in [20] and the result compares well with the measured anomalous dispersion.

All these findings support a generic nature of the OBSM phonon anomalies in the HTSCs. The frequency renormalization and a corresponding increase of the linewidths point to a strong coupling of these phonons to the charge carriers. Deviations from the presumably generic dispersion for the OBSM in the form of a sharp softening have recently been reported in inelastic neutron scattering (INS) and high resolution inelastic x-ray scattering (IXS) experiments, respectively, for $La_{2-x}Ba_xCuO_4$ at $x = 0.125$ [6] and $x = 0.14$ [21]. This has been related to the possibility of stripe formation in this compound.

According to our calculations the origin of the phonon anomalies is a strong *nonlocal* EPI due to specific screening

 

effects in the form of a polarization created by metallic charge fluctuations (CFs) on the outer shells of the Cu and $O_{xy}$ ions in the CuO plane; see, e.g., [22–24]. This type of screening characteristic for a strongly inhomogeneous electronic system like the cuprates with a strong component of ionic binding and a corresponding density distribution which is mainly concentrated at the ions in the CuO plane leads for the p-doped cuprates [22, 24] and also for the n-doped $Nd_2CuO_4$ [20] to an anomalous behavior of the dispersion.

The specific form of screening yields for the OBSM in metallic $La_2CuO_4$ and $Nd_2CuO_4$ a *downward* dispersion of the anomalous longitudinal branch with high frequencies along the (1, 0, 0) and the (1, 1, 0) directions, respectively. In the case of $Nd_2CuO_4$, however, the dispersion of the branches with high frequencies comprising the anomalous OBSM is more complex than in $La_2CuO_4$ because there are, in contrast to $La_2CuO_4$, several branches of the same symmetry type nearby in energy, leading to complex anticrossing phenomena [20]. Such a possibility is also investigated for $HgBa_2CuO_4$ and $Bi_2Sr_2CuO_6$ in this work.

The anomalous dispersion cannot be understood within a typical lattice dynamical model, like the shell model, extended by a homogeneous electron gas screening that is *diagonal* in reciprocal space. This type of dielectric response always yields an *increasing* dispersion when passing from the center of the Brillouin zone (BZ) into the zone, because of an incomplete screening of the phonon-induced changes of the Coulomb potential at shorter distances. In contrast, the anomalous softening of the OBSM in particular of the oxygen half-breathing mode ($\Delta_1/2$ anomaly halfway along the $\Delta \sim (1, 0, 0)$ direction) and the full oxygen breathing mode ($O_B^X$ at the X point of the BZ) is a result of an 'overscreening' of the phonon-induced changes of the Coulomb potential. The overscreening effect has been shown by our calculations to be due to nonlocally excited CFs localized at the Cu and $O_{xy}$ sites in the CuO plane accompanied by (dynamic) charge ordering in the form of localized stripes of alternating sign in the plane [22, 25]. Expressed in terms of the density response matrix in reciprocal space such a strong nonlocal EPI effect and 'overscreening' of the OBSM is related to the *off-diagonal elements* (local field effect) being apparently very important in the cuprates, as revealed by the anomalous softening found in our studies.

In our calculations a sufficiently broad set of orbital degrees of freedom (Cu 3d, Cu 4s, O 2p), the full three-dimensional long range Coulomb interaction as well as the short range local repulsion of the electrons, especially the important on-site repulsion mediated by the localized Cu 3d orbital, is considered quantitatively. All the resulting couplings arising in the dynamical matrix are microscopically well defined and can be calculated.

From our investigations, see, e.g., [26], we extract a strong EPI for the phonon anomalies $\Delta_1/2$ and $O_B^X$, which can be well treated in an *adiabatic* approximation. Moreover, we find a very strong nonadiabatic enhancement of the coupling compared to the adiabatic case for phonon-like modes, like $O_z^Z$ (axial oxygen breathing mode at the Z point of the BZ), from a small *nonadiabatic* region around the $c$ axis. In this region poor dynamical screening due to the slow charge dynamics around the $c$ axis of the long range polar Coulomb interaction of the ions leads in metallic $LaCuO_4$ to low-energy plasmons mixing with certain interlayer phonons of the same symmetry. For a discussion of phonon–plasmon mixing in the cuprates, see also [27]. An essential nonlocal interaction of holes with $c$-axis-polarized optical phonons in the HTSCs has also been reported in [28, 29].

Our calculations show that, besides the more delocalized Cu 4s state, the short range part of the Coulomb interaction $U_d$ related to the localized Cu 3d orbital is particular important for the $\Delta_1/2$ and $O_B^X$ mode polarized and propagating in the CuO plane while the strong long range nonlocal polar Coulomb interaction plays an important role for $O_z^Z$ and similar $\Lambda_1$ phonons polarized and propagating along the $c$ axis. Thus, the relevance of both short range electron repulsion $U_d$ in the correlated Cu 3d state as well as long range polar coupling of the electrons to the phonons is demonstrated by our calculations of the phonon anomalies in the cuprates. Consequently, any quantitative study of the physics of the normal or superconducting state of the cuprates should consider electron correlations and strong nonlocal EPI on an equal footing.

This paper is organized as follows. In section 2 the theory and modeling is briefly reviewed. Section 3 presents the calculations for the phonon dynamics, charge response and phonon density of states of $HgBa_2CuO_4$ and $Bi_2Sr_2CuO_6$ and a comparison with earlier calculations of $LaCuO_4$ and $Nd_2CuO_4$. The main focus is on the OBSM phonon anomalies in the various materials and the effect of the charge response in the ionic layers on the dispersion. A summary of the paper is given in section 4 and the conclusions are drawn.

## 2. Theory and modeling

In the following a brief survey of the theory and modeling is presented. A detailed description can be found in [23] and in particular in [30] where the calculation of the coupling parameters of the theory is presented.

The local part of the electronic charge response and the EPI is approximated in the spirit of the *quasi-ion approach* [20, 31] by an *ab initio* rigid-ion model (RIM), taking into account covalent ion softening in terms of (static) effective ionic charges calculated from a tight-binding analysis. The tight-binding analysis supplies these charges as extracted from the orbital occupation numbers $Q_\mu$ of the $\mu$ (tight-binding) orbital in question:

$$Q_\mu = \frac{2}{N} \sum_{n\mathbf{k}} |C_{\mu n}(\mathbf{k})|^2. \tag{1}$$

$C_{\mu n}(\mathbf{k})$ stands for the $\mu$ component of the eigenvector of band $n$ at the wavevector $\mathbf{k}$ in the first BZ; the summation in equation (1) runs over all occupied states and $N$ gives the number of elementary cells in the (periodic) crystal.

In addition, scaling of the short range part of certain pair potentials between the ions is performed to simulate further covalence effects in the calculation in such a way that

the energy-minimized structure is as close as possible to the experimental one [32]. Structure optimization and energy minimization is very important for a reliable calculation of the phonon dynamics through the dynamical matrix. Taking just the experimental structure data as is done in many cases in the literature may lead to uncontrolled errors in the phonon calculations.

The RIM with the corrections just mentioned then serves as an unbiased reference system for the description of the HTSCs and can be considered as a first approximation for the insulating state of these compounds because of the strong ionic nature of bonding in the cuprates. Starting with such an unprejudiced rigid reference system non-rigid electronic polarization processes are introduced in the form of more or less localized electronic charge fluctuations (CFs) at the outer shells of the ions. Especially in the metallic state of the HTSCs the latter dominate the *nonlocal* contribution of the electronic density response and the EPI and are particularly important in the CuO planes. In addition, *anisotropic* dipole fluctuations (DFs) are admitted in our approach [30, 33]. They prove to be specifically of interest for the ions in the ionic layers mediating the dielectric coupling and for the polar modes. Thus, the basic variable of our model is the ionic density which is given in the perturbed state by

$$\rho_\alpha(\mathbf{r}, Q_\lambda, \mathbf{p}_\alpha) = \rho_\alpha^0(r) + \sum_\lambda Q_\lambda \rho_\lambda^{\mathrm{CF}}(r) + \mathbf{p}_\alpha \cdot \hat{\mathbf{r}} \rho_\alpha^{\mathrm{D}}(r). \quad (2)$$

$\rho_\alpha^0$ is the density of the unperturbed ion, as used in the RIM, localized at the sublattice $\alpha$ of the crystal and moving rigidly with the latter under displacement. The $Q_\lambda$ and $\rho_\lambda^{\mathrm{CF}}$ describe the amplitudes and the form factors of the CFs and the last term in equation (2) represents the dipolar deformation of an ion $\alpha$ with amplitude (dipole moment) $\mathbf{p}_\alpha$ and a radial density distribution $\rho_\alpha^{\mathrm{D}}$. $\hat{\mathbf{r}}$ denotes the unit vector in the direction of $\mathbf{r}$. The $\rho_\lambda^{\mathrm{CF}}$ are approximated by a spherical average of the orbital densities of the ionic shells calculated in the LDA taking self-interaction effects (SIC) into account. The dipole density $\rho_\alpha^{\mathrm{D}}$ is obtained from a modified Sternheimer method in the framework of LDA-SIC [30]. All SIC calculations are performed for the average spherical shell in the orbital-averaged form according to Perdew and Zunger [34]. For the correlation part of the energy per electron the parameterization given in [34] has been used.

The total energy of the crystal is obtained by assuming that the density can be approximated by a superposition of overlapping densities $\rho_\alpha$. The $\rho_\alpha^0$ in equation (2) are also calculated within the LDA-SIC, taking environment effects, via a Watson sphere potential and the calculated static effective charges of the ions, into account. The Watson sphere method is only used for oxygen ions and the depth of the Watson sphere potential is set as the Madelung potential at the corresponding site. Such an approximation holds well in the HTSCs [32, 35]. Finally, applying the pair-potential approximation we get for the total energy

$$E(R, \zeta) = \sum_{\mathbf{a},\alpha} E_\alpha^{\mathbf{a}}(\zeta) + \tfrac{1}{2} \sum_{(\mathbf{a},\alpha)\neq(\mathbf{b},\beta)} \Phi_{\alpha\beta}\left(\mathbf{R}_\beta^{\mathbf{b}} - \mathbf{R}_\alpha^{\mathbf{a}}, \zeta\right). \quad (3)$$

The energy $E$ depends on both the configuration of the ions $\{R\}$ and the electronic (charge) degrees of freedom (EDF) $\{\zeta\}$ of the charge density, i.e. $\{Q_\lambda\}$ and $\{\mathbf{p}_\alpha\}$ in equation (2). $E_\alpha^{\mathbf{a}}$ are the energies of the single ions. **a** and **b** denote the elementary cells, and $\alpha$ and $\beta$ the corresponding sublattices. The second term in equation (3) is the interaction energy of the system, expressed in terms of *anisotropic* pair interactions $\Phi_{\alpha\beta}$. Both $E_\alpha^{\mathbf{a}}$ and $\Phi_{\alpha\beta}$ in general depend upon $\zeta$ via $\rho_\alpha$ in equation (2).

The pair potentials in equation (3) can be separated into long range Coulomb contributions and short range terms; for details see, e.g., [30].

From the adiabatic condition

$$\frac{\partial E(R, \zeta)}{\partial \zeta} = 0 \quad (4)$$

the electronic degrees of freedom $\zeta$ can be eliminated, an expression for the atomic force constants can be given and from this the dynamical matrix in the harmonic approximation can be derived as

$$t_{ij}^{\alpha\beta}(\mathbf{q}) = [t_{ij}^{\alpha\beta}(\mathbf{q})]_{\mathrm{RIM}} - \frac{1}{\sqrt{M_\alpha M_\beta}} \sum_{\kappa,\kappa'} [B_i^{\kappa\alpha}(\mathbf{q})]^* [C^{-1}(\mathbf{q})]_{\kappa\kappa'} B_j^{\kappa'\beta}(\mathbf{q}). \quad (5)$$

The first term on the right-hand side denotes the contribution from the RIM. $M_\alpha$, $M_\beta$ are the masses of the ions and $\mathbf{q}$ is a wavevector from the first BZ.

The quantities $\mathbf{B}(\mathbf{q})$ and $C(\mathbf{q})$ in equation (5) represent the Fourier transforms of the electronic coupling coefficients and are calculated from the energy in equation (3), i.e.

$$\mathbf{B}_{\kappa\beta}^{\mathbf{ab}} = \frac{\partial^2 E(R, \zeta)}{\partial \zeta_\kappa^{\mathbf{a}} \partial R_\beta^{\mathbf{b}}}, \quad (6)$$

$$C_{\kappa\kappa'}^{\mathbf{ab}} = \frac{\partial^2 E(R, \zeta)}{\partial \zeta_\kappa^{\mathbf{a}} \partial \zeta_{\kappa'}^{\mathbf{b}}}. \quad (7)$$

$\kappa$ denotes the EDF (CF and DF in the present model, see equation (2)) in an elementary cell. The **B** coefficients describe the coupling between the EDF and the displaced ions (bare electron–phonon coupling), and the coefficients $C$ determine the interaction between the EDF. The phonon frequencies $\omega_\sigma(\mathbf{q})$ and the corresponding eigenvectors $\mathbf{e}^\alpha(\mathbf{q}\sigma)$ of the modes $(\mathbf{q}\sigma)$ are obtained from the secular equation for the dynamical matrix in equation (5), i.e.

$$\sum_{\beta,j} t_{ij}^{\alpha\beta}(\mathbf{q}) e_j^\beta(\mathbf{q}) = \omega^2(\mathbf{q}) e_i^\alpha(\mathbf{q}). \quad (8)$$

Equations (5)–(8) are generally valid and, in particular, are independent of the specific model for the decomposition of the perturbed density in equation (2) and the pair approximation in equation (3) for the energy. The lengthy details of the calculation of the coupling coefficients **B** and $C$ cannot be reviewed in this paper. They are presented in [30]. In this context we note that the coupling matrix $C_{\kappa\kappa'}(\mathbf{q})$ of the EDF–EDF interaction, whose inverse appears in equation (5) for the dynamical matrix, can be written in matrix notation as

$$C = \Pi^{-1} + \tilde{V}. \quad (9)$$

$\Pi^{-1}$ is the inverse of the *proper polarization part* of the density response matrix and contains the kinetic part to the interaction $C$ while $\tilde{V}$ embodies the Hartree and exchange–correlation contribution, because they are related to the second functional derivatives with respect to the density $\rho$ of the kinetic energy and the exchange–correlation energy, respectively [23]. $C^{-1}$ needed for the dynamical matrix and the EPI is closely related to the linear density response matrix and to the inverse dielectric matrix $\varepsilon^{-1}$, respectively.

Only a very few attempts have been made to calculate the phonon dispersion and the EPI of the HTSCs using the linear response method in the form of density functional perturbation theory (DFPT) within LDA [36–39]. These calculations correspond to calculating $\Pi$ and $\tilde{V}$ in DFT-LDA and for the *metallic* state only. On the other hand, in our microscopic modeling DFT-LDA-SIC calculations are performed for the various densities in equation (2) in order to obtain the coupling coefficients **B** and $\tilde{V}$. Including SIC is particularly important for localized orbitals like Cu 3d in the HTSCs. Our theoretical results for the phonon dispersion [22, 24, 26, 33], which compare well with the experiments, demonstrate that the approximative calculation of the coupling coefficients in our approach is sufficient, even for the localized Cu 3d states. Written in matrix notation we get for the density response matrix the relation

$$C^{-1} = \Pi(1 + \tilde{V}\Pi)^{-1} \equiv \Pi\varepsilon^{-1}, \qquad \varepsilon = 1 + \tilde{V}\Pi. \quad (10)$$

The CF–CF submatrix of the matrix $\Pi$ can approximately be calculated for the metallic (but not for the undoped and underdoped) state of the HTSCs from a TBA of a single-particle electronic band structure. In this case the electronic polarizability $\Pi$ in a tight-binding representation is

$$\Pi_{\kappa\kappa'}(\mathbf{q}, \omega = 0) = -\frac{2}{N}\sum_{n,n',\mathbf{k}} \frac{f_{n'}(\mathbf{k}+\mathbf{q}) - f_n(\mathbf{k})}{E_{n'}(\mathbf{k}+\mathbf{q}) - E_n(\mathbf{k})} \times [C^*_{\kappa n}(\mathbf{k})C_{\kappa n'}(\mathbf{k}+\mathbf{q})][C^*_{\kappa' n}(\mathbf{k})C_{\kappa' n'}(\mathbf{k}+\mathbf{q})]^*. \quad (11)$$

$f$, $E$ and $C$ in equation (11) are the occupation numbers, the single-particle energies and the expansion coefficients of the Bloch functions in terms of tight-binding functions.

The self-consistent change of an EDF at an ion induced by a phonon mode $(\mathbf{q}\sigma)$ with frequency $\omega_\sigma(\mathbf{q})$ and eigenvector $\mathbf{e}^\alpha(\mathbf{q}\sigma)$ can be derived in the form

$$\delta\zeta^{\mathbf{a}}_\kappa(\mathbf{q}\sigma) = \left[-\sum_\alpha \mathbf{X}^{\kappa\alpha}(\mathbf{q})\mathbf{u}_\alpha(\mathbf{q}\sigma)\right] e^{i\mathbf{q}\mathbf{R}^{\mathbf{a}}_\kappa} \equiv \delta\zeta_\kappa(\mathbf{q}\sigma)e^{i\mathbf{q}\mathbf{R}^{\mathbf{a}}}, \quad (12)$$

with the displacement of the ions

$$\mathbf{u}^{\mathbf{a}}_\alpha(\mathbf{q}\sigma) = \left(\frac{\hbar}{2M_\alpha\omega_\sigma(\mathbf{q})}\right)^{1/2} \mathbf{e}^\alpha(\mathbf{q}\sigma)e^{i\mathbf{q}\mathbf{R}^{\mathbf{a}}} \equiv \mathbf{u}_\alpha(\mathbf{q}\sigma)e^{i\mathbf{q}\mathbf{R}^{\mathbf{a}}}. \quad (13)$$

The self-consistent response per unit displacement of the EDF in equation (12) is calculated in linear response theory as

$$\mathbf{X}(\mathbf{q}) = \Pi(\mathbf{q})\varepsilon^{-1}(\mathbf{q})\mathbf{B}(\mathbf{q}) = C^{-1}(\mathbf{q})\mathbf{B}(\mathbf{q}). \quad (14)$$

The generalization for the quantity $\Pi$ in equations (9) and (10) needed for the kinetic part of the charge response in the nonadiabatic regime, where dynamical screening effects must be considered, can be achieved by adding $(\hbar\omega + i\eta)$ to the differences of the single-particle energies in the denominator of the expression for $\Pi$ in equation (11). Other possible nonadiabatic contributions to $C$ related to dynamical exchange–correlation effects and the phonons themselves are beyond the scope of the present approach. Using equation (10) for the dielectric matrix, $\varepsilon$, and the frequency-dependent version of the irreducible polarization part, $\Pi$, according to equation (11), the free-plasmon dispersion is obtained from the condition

$$\det[\varepsilon_{\kappa\kappa'}(\mathbf{q}, \omega)] = 0. \quad (15)$$

The coupled-mode frequencies of the phonons and the plasmons must be determined self-consistently from the secular equation (8) for the dynamical matrix which now contains the frequency $\omega$ implicitly via $\Pi$ in the response function $C^{-1}$. Such a nonadiabatic approach is necessary for a description of the interlayer phonons and the charge response within a small region around the $c$ axis as performed in [22, 26].

**Table 1.** Static effective charges of the ions.

| $La_2CuO_4$ | $Nd_2CuO_4$ | $HgBa_2CuO_4$ | $Bi_2Sr_2CuO_6$ |
|---|---|---|---|
| La: 2.28+ | Nd: 2.35+ | Hg: 1.44+ | Bi: 2.28+ |
| | | Ba: 1.69+ | Sr: 1.85+ |
| Cu: 1.22+ | Cu: 1.22+ | Cu: 1.70+ | Cu: 1.22+ |
| $O_{xy}$: 1.42− | $O_{xy}$: 1.42− | $O_{xy}$: 1.56− | $O_{xy}$: 1.42− |
| $O_z$: 1.47− | $O_z$: 1.54− | $O_z$: 1.70− | $O_z$: 1.47− |
| | | | O3: 1.85− |

## 3. Results and discussion

### 3.1. Ionic reference system and structural data

For a definitive discussion of the renormalization of the phonon modes introduced by the nonlocal EPI effects related to the electronic polarization processes of CF and DF type, a quantitative reference model for the calculation of the phonon dispersion based essentially on the important component of ionic binding is necessary. A suitable model sketched in section 2 which represents approximately the local EPI effects is provided by the *ab initio* rigid-ion model, extended by covalent ion softening and scaling of the short range part of certain pair potentials.

A modified ionic description is quite generally a good starting point for the physics in the cuprates, in particular for their insulating state. In this context we also refer to the work in [40–42]. In our calculations we found a suitable set of static effective charges given in table 1 which, together with covalent scaling, leads to a good overall agreement with the experimental structural data shown in table 2. The charges of the Cu and the $O_{xy}$ ions in the CuO plane are taken to be identical for $La_2CuO_4$, $Nd_2CuO_4$ and $Bi_2Sr_2CuO_6$. They result from a tight-binding analysis of the *ab initio* band structure in $La_2CuO_4$ [32]. This means that the CuO plane is treated as generic for these materials as far as the effective charges are concerned. On the other hand, for $HgBa_2CuO_4$ these

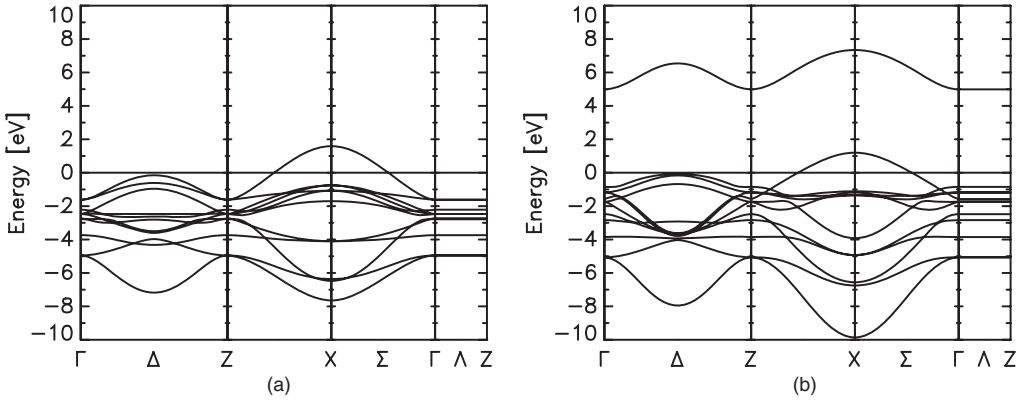


**Figure 1.** Electronic band structure of the (a) 11BM and (b) 12BM.

**Table 2.** Structural data for the investigated compounds. For each lattice parameter, the first row shows the calculated data and the second row the experimental data in brackets. The lattice constants $a$ and $c$ and the distances between the ions are given in units of Å, while the relative translation $\tau$ is in units of $c$. In $Nd_2CuO_4$, $\tau(O_z)$ is fixed by symmetry. The experimental references are listed following the name of the compounds.

| $La_2CuO_4$ [43] | $Nd_2CuO_4$ [44] | $HgBa_2CuO_4$ [45] | $Bi_2Sr_2CuO_6$ [46] |
|---|---|---|---|
| $a = 3.763$ | $a = 4.155$ | $a = 3.8995$ | $a = 3.741$ |
| (3.810) | (3.945) | (3.875) | (3.798) |
| $c = 13.197$ | $c = 12.102$ | $c = 9.521$ | $c = 23.490$ |
| (13.240) | (12.171) | (9.513) | (24.662) |
| $c/a = 3.5$ | $c/a = 2.9$ | $c/a = 2.4$ | $c/a = 6.3$ |
| (3.5) | (2.9) | (2.5) | (6.5) |
| $\tau(O_z) = 0.185$ | $\tau(O_z) = 0.250$ | $\tau(O_z) = 0.313$ | $\tau(O_z) = 0.109$ |
| (0.182) | (0.250) | (0.294) | (0.105) |
| $\tau(La) = 0.134$ | $\tau(Nd) = 0.153$ | $\tau(Ba) = 0.183$ | $\tau(O3) = 0.199$ |
| (0.138) | (0.149) | (0.198) | (0.186) |
| | | | $\tau(Bi) = 0.189$ |
| | | | (0.184) |
| | | | $\tau(Sr) = 0.068$ |
| | | | (0.071) |
| $Cu–O_{xy} = 1.881$ | $Cu–O_{xy} = 2.078$ | $Cu–O_{xy} = 1.950$ | $Cu–O_{xy} = 1.870$ |
| (1.895) | (1.972) | (1.940) | (1.896) |
| $Cu–O_z = 2.441$ | $Cu–O_z = 3.670$ | $Cu–O_z = 2.980$ | $Cu–O_z = 2.556$ |
| (2.407) | (3.622) | (2.793) | (2.585) |
| $O_z$–La = 2.382 | $O_z$–Nd = 2.389 | $O_z$–Hg = 1.800 | $O_z$–Bi = 1.893 |
| (2.381) | (2.323) | (1.966) | (1.944) |

charges have to be chosen to be more ionic, otherwise the phonon modes are too low in frequency as compared with the experiment. In all the materials covalent scaling of the short range pair potential between the Cu and the $O_{xy}$ ions in the plane is very essential and in the case of $HgBa_2CuO_4$ and $Bi_2Sr_2CuO_6$ in addition between the apex oxygen $O_z$ and Hg and $O_z$ and Bi, respectively.

This is consistent with a significantly shorter distance of the $O_z$–Hg and $O_z$–Bi link as compared to $O_z$–La or $O_z$–Nd in $La_2CuO_4$ and $Nd_2CuO_4$, respectively ($O_z$–Hg: 1.97 Å; $O_z$–Bi: 1.94 Å; $O_z$–La: 2.38 Å; $O_z$–Nd: 2.32 Å). Thus, the overlap of the orbital densities in the $O_z$–Hg and $O_z$–Bi bond is sufficiently large and consequently metallic CFs between the partially occupied $O_z$ 2p and Hg 6s orbitals and the $O_z$ 2p and Bi 6p orbitals, respectively, can be expected. The important effect of such CFs on certain phonon modes will be discussed in section 3.2.

### *3.2. Phonon dispersion, charge response and phonon density of states*

The calculation of the phonon dispersion in this section is based on the dynamical matrix given in equation (5) within the adiabatic approximation which has been shown to be a good approximation for all phonon modes outside a small region around the $c$ axis, where, on the other hand, a nonadiabatic approach is necessary [22, 26]. As discussed, e.g. [26], the nonadiabatic region around the $c$ axis is so small that it cannot be resolved by INS experiments or other probes so far. Thus, only an average of the dispersion can be measured along the $\Lambda \sim (0, 0, 1)$ direction for modes of $\Lambda_1$ symmetry because of their coupling to a low lying $c$-axis plasmon as discussed in [26]. Consequently, all results for the $\Lambda_1$ phonons propagating and polarized along the $c$ axis calculated in the adiabatic approximation or reported in the experiments must be interpreted as an average over the small region with a nonadiabatic charge response.

Anisotropic DFs being particular important along the $c$ axis and for ions in the ionic layers [20, 33, 47] have been taken into account in all computations of the phonon modes in this paper.

The subsequent calculations are representative of the well-doped metallic state of the materials where a fully developed Fermi surface exists. Investigations of the charge response and phonon dynamics of the underdoped pseudogap state and the insulating state of the cuprates have been performed in [20, 24, 33]. These calculations are based on a microscopic modeling of the electronic polarizability in terms of rigorous orbital specific compressibility–incompressibility sum rules for $\Pi_{\kappa\kappa'}(\mathbf{q})$ in the long wavelength limit in order to discriminate between the charge response of the different electronic states of the cuprates.

In the following we discuss the effect of the renormalization of the phonon dispersion by metallic CFs which are of particular importance for the anomalous high-frequency oxygen bond-stretching modes OBSM. In our earlier calculations of the phonon anomalies and the phonon dispersion of $La_2CuO_4$ and $Nd_2CuO_4$ [20, 24, 33, 48] we have applied successfully a parameterized description ($\Pi$ model) for the electronic polarizability matrix $\Pi_{\kappa\kappa'}$ in equation (11). This model highlights, besides the effect of the localized Cu 3d state, the importance of the delocalized Cu 4s component in the charge response and for the softening of the anomalous OBSM phonon modes. The importance of the Cu 4s orbital for a realistic description of the electronic structure of the HTSCs has also been pointed out in [49, 50].

In order to demonstrate selectively the renormalization effect introduced by the Cu 4s orbital for the OBSM not only within the $\Pi$-model approach. we have calculated $\Pi_{\kappa\kappa'}$ approximately using for the electronic band structure of the CuO plane an eleven-band model (11BM: based on Cu 3d and O 2p states [51]) and a twelve-band model (12BM) which takes the Cu 4s state into account in addition.

In figure 1 the result for the electronic band structure of the 11BM and the 12BM is displayed and in figure 2 the corresponding results for the OBSM phonon anomalies are shown for the case of $La_2CuO_4$. The important contribution of the Cu 4s degree of freedom in the charge response for the anomalies is evident by inspection of the dotted and broken curve in figure 2. The full curve relies on a diagonal $\Pi$ model [48], where the matrix elements of the polarizability matrix $\Pi(\text{Cu 3d}) = 2.8\ \text{eV}^{-1}$, $\Pi(\text{Cu 4s}) = 0.055\ \text{eV}^{-1}$ and $\Pi(\text{O}_{xy}\ \text{2p}) = 0.2\ \text{eV}^{-1}$ have been extracted from the full polarizability matrix, as obtained from a tight-binding analysis of the electronic band structure for $La_2CuO_4$ (31BM [52]) within the framework of the local density approximation (LDA) of density functional theory (DFT). The value for $\Pi(\text{Cu } 4s)$, however, has been slightly increased compared with the 31BM from 0.05 to 0.055 $\text{eV}^{-1}$ in order to optimize the calculated result for the $\Delta_1$ branch in comparison to the experiment.

Using the 11BM or 12BM, respectively, as generic models for the electronic structure of the CuO plane also in the calculation of the phonon dispersion of $Nd_2CuO_4$, $HgBa_2CuO_4$ and $Bi_2Sr_2CuO_6$ we find that the softening of the OBSM due to the Cu 4s CFs is of the same size as for $La_2CuO_4$ displayed in figure 2.

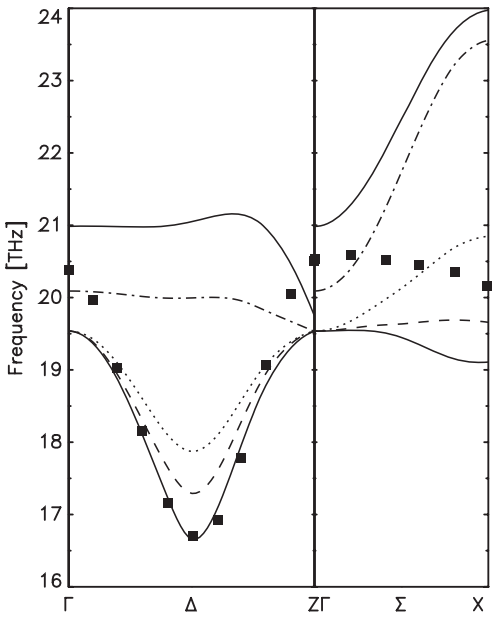


**Figure 2.** Calculated OBSM phonon anomalies in $La_2CuO_4$: RIM (— · · —), RIM with anisotropic DFs (— · —), 11BM (· · · · · ·), 12BM (– – –) and $\Pi$ model (——). The squares (■) represent experimental results [9].

The detailed results for the renormalization of the OBSM are shown in figure 3 where the displacement patterns of the half-breathing mode ($\Delta_1/2$ anomaly) and the full-breathing mode $O_B^X$ are given. Moreover, we have listed the corresponding frequencies in THz as calculated in the RIM, the 11BM and the 12BM. It should be noted that, due to the simple tetragonal elementary cell, in $HgBa_2CuO_4$ the full-breathing mode is located at M and the half-breathing mode at X, but to be consistent with the other three compounds we keep the notation $\Delta_1/2$ and $O_B^X$ also for $HgBa_2CuO_4$.

A measure of the electron–phonon coupling strength is given by the mode- and orbital-selective charge fluctuations $\delta\zeta_\kappa(\mathbf{q}\sigma)$ from equation (12) and the related renormalization of the corresponding phonon modes. We find a very strong renormalization of the mode frequencies by the electronic polarization processes which nearly exclusively result from the nonlocally excited CFs $\delta\zeta_\kappa$ listed in table 3. The softening for $O_B^X$ as compared to the RIM is in the range between 4 and 5 THz and for $\Delta_1/2$ between 2 and 4 THz. The largest softening for $\Delta_1/2$ occurs in $La_2CuO_4$ partly due to the fact that there is virtually no anticrossing with other modes of $\Delta_1$ symmetry.

The significant renormalization of the OBSM in all the compounds investigated so far signals a strong nonlocal electron–phonon coupling in the cuprates. This strong coupling, in particular the effect of the Cu 4s orbital, can also be read off from the calculated magnitude of the phonon-induced charge response given in table 3 in terms of the CFs $\delta\zeta_\kappa(\mathbf{q}\sigma)$ according to equation (12).

Our calculations for $HgBa_2CuO_4$ and $Bi_2Sr_2CuO_6$ in the following are based on the $\Pi$-model approach because

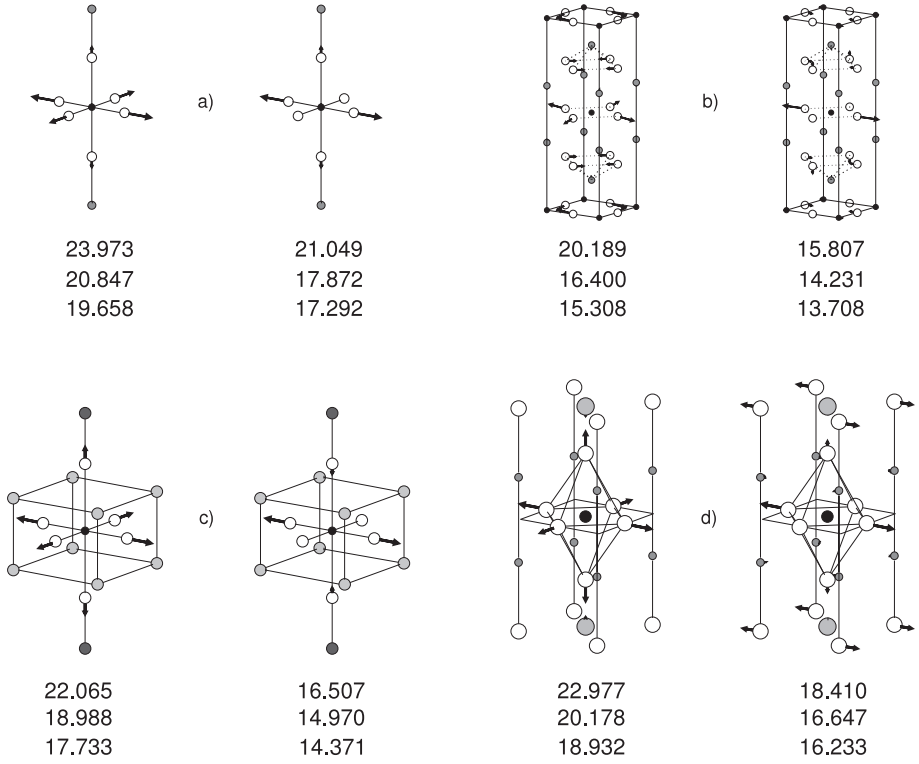


**Figure 3.** Displacement patterns of the OBSM for (a) $La_2CuO_4$, (b) $Nd_2CuO_4$, (c) $HgBa_2CuO_4$ and (d) $Bi_2Sr_2CuO_6$. The left pattern shows $O_B^X$ and the right pattern $\Delta_1/2$, respectively. For each displacement pattern the phonon frequency is given for the RIM (first row), the 11BM (second row) and the 12BM (third row) in units of THz.

**Table 3.** Magnitudes of the calculated charge CFs $\delta\zeta_\kappa$ in units of $10^{-3}$ particles for the breathing and half-breathing modes. In the first row the values for the 11BM are given, while the second row shows the values for the 12BM, respectively. The symbol / means, that CFs are not allowed in the model and − means CFs are not excited for symmetry reasons. The corresponding displacement patterns are shown in figure 3.

| | Cu 3d | Cu 4s | $O_y$ 2p | Cu 3d | Cu 4s | $O_y$ 2p |
|---|---|---|---|---|---|---|
| | $La_2CuO_4$ | | | $Nd_2CuO_4$ | | |
| $O_B^X$ | −23.216 | / | − | −18.860 | / | − |
| | −19.949 | −13.255 | − | −16.976 | −13.129 | − |
| $\Delta_1/2$ | −16.946 | / | −6.520 | −14.221 | / | −5.666 |
| | −15.393 | −8.685 | −3.283 | −13.284 | −8.473 | −3.152 |
| | $HgBa_2CuO_4$ | | | $Bi_2Sr_2CuO_6$ | | |
| $O_B^X$ | −24.231 | / | − | −22.078 | / | − |
| | −17.100 | −13.576 | − | −17.081 | −11.575 | − |
| $\Delta_1/2$ | −17.528 | / | −8.865 | −13.881 | / | −8.756 |
| | −16.276 | −9.228 | −5.904 | −11.955 | −6.473 | −4.002 |

unlike $La_2CuO_4$ no reliable tight-binding parameterization of a first-principles band structure is available for these compounds. Even if a tight-binding parameterization of a typical DFT-LDA-based band structure would exist it would not be sufficient to describe the dynamics of the $\Lambda_1$ modes in the HTSC polarized and propagating along the $c$ axis. This is because typical DFT-LDA calculations are much too isotropic and underestimate the anisotropy of the real materials by far too much. For a detailed discussion of this interesting topic in the case of $La_2CuO_4$ and its relevance for the nonadiabatic charge response and the related phonon–plasmon mixing, see [26, 53]. A short comment should be made concerning the size of the electron–phonon coupling strength of the adiabatic OBSM with amplitudes within the plane ($\Delta_1/2$, $O_B^X$) compared to modes with out-of-plane amplitudes as the nonadiabatic apex oxygen bond stretching mode $O_z^Z$. Like in the present paper in our calculations for $La_2CuO_4$ [26] an already strong coupling of the adiabatic modes $\Delta_1/2$ and $O_B^X$ has been found. However, for the nonadiabatic $O_z^Z$ mode with out-of-plane amplitudes we obtain in addition a very strong increase of the coupling as compared to the adiabatic in-plane modes.

Phonon–plasmon mixing in the nonadiabatic region around the $c$ axis provides an extra channel for the formation of Cooper pairs. For a suitable strength of interlayer coupling it becomes possible to achieve large contributions to the coupling from both the phonon-like and the plasmon-like modes, as discussed in [22, 55]. Assuming that the phonon–plasmon contribution to pairing is significant this finding could help in the search of new high-$T_c$ materials. This can be accomplished by changing the out-of-plane solid-state chemistry in order to tune the interlayer coupling.

Within our Π-model approach we can model the charge response for ions out of the CuO plane by adjusting the corresponding polarizability matrix elements of these ions in order to obtain a reasonable description of the frequency of certain phonon modes which are most sensitive to the charge response of the most important out-of-plane ions. So, as a first approximation we take the Π model for the CuO plane

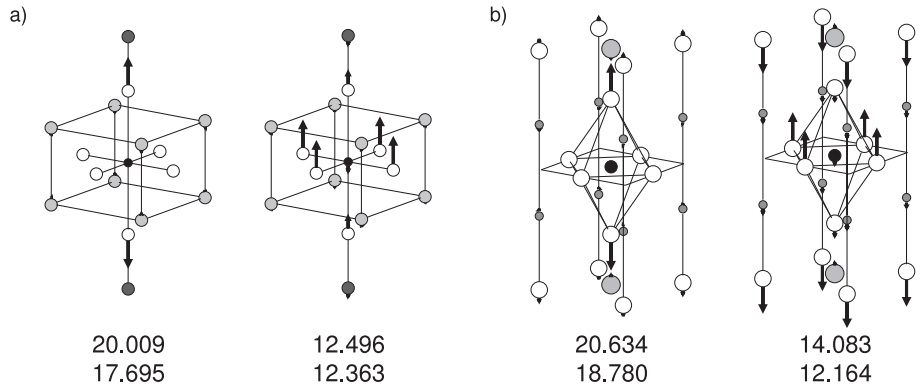


**Figure 4.** Displacement patterns of selected optical modes for (a) $HgBa_2CuO_4$ and (b) $Bi_2Sr_2CuO_6$. The left pattern shows the Raman-active $O_z^\Gamma$ mode and the right pattern the infrared-active $A_{2u}$ mode discussed in the text, respectively. For each displacement pattern the phonon frequency is given for model Π-2dim (first row) and model Π-3dim (second row) in units of THz.

**Table 4.** Frequencies of the calculated and experimental measured Raman- and infrared-active modes in units of THz.

| $HgBa_2CuO_4$ | $A_{1g}$ | $A_{1g}$ ($O_z^\Gamma$) | $E_g$ | $E_g$ | $A_{2u}$ | $A_{2u}$ | $A_{2u}$ | $A_{2u}$ | |
|---|---|---|---|---|---|---|---|---|---|
| Π-2dim | 5.17 | 20.01 | 2.61 | 4.20 | 3.44 | 4.87 | 12.50 | 17.55 | |
| Π-3dim | 4.63 | 17.70 | 2.61 | 4.20 | 3.31 | 4.86 | 12.36 | 17.32 | |
| Exp. [56] | 4.83 | 17.75 | 2.25 | 5.04 | | | | | |
| Exp. [59] | | | | | 2.58 | 4.50 | 10.67 | 18.80 | |
| $Bi_2Sr_2CuO_6$ | $A_{1g}$ | $A_{1g}$ | $A_{1g}$ | $A_{1g}$ ($O_z^\Gamma$) | $A_{2u}$ | $A_{2u}$ | $A_{2u}$ | $A_{2u}$ | $A_{2u}$ |
| Π-2dim | 4.18 | 7.02 | 14.06 | 20.63 | 2.99 | 5.09 | 9.25 | 14.08 | 18.67 |
| Π-3dim | 4.16 | 5.89 | 13.59 | 18.78 | 2.79 | 5.08 | 9.17 | 12.16 | 18.10 |
| Exp. [57] | 2.07 | 3.57 | 13.61 | 18.71 | | | | | |
| Exp. [58] | 3.60 | 6.00 | 13.76 | 18.74 | | | | | |
| Exp. [60] | | | | | 3.27 | 4.95 | 9.02 | 11.54 | 17.57 |

as introduced for $La_2CuO_4$ above also for $HgBa_2CuO_4$ and $Bi_2Sr_2CuO_6$. From table 4 a comparison of the calculated frequencies of the Raman modes with experiment shows that the largest difference between theory and experiment appears for the Raman mode $O_z^\Gamma$ with the highest frequency. Here the apex oxygen ion vibrates along the $c$ axis against the Hg or Bi ions, respectively, which are located just above the apex oxygen, see figure 4. As already mentioned in section 3.1 there is a relatively short distance between $O_z$ and Hg or Bi, respectively, and consequently metallic CFs can be expected which should renormalize the corresponding modes.

In order to investigate this effect we extend the Π model for the CuO plane (Π-2dim) by allowing for metallic charge fluctuations on the $O_z$, Hg and Bi ions (Π-3dim). The corresponding matrix elements Π(Hg 6s) and Π($O_z$ 2p), for $HgBa_2CuO_4$ and Π(Bi 6p), Π($O_z$ 2p) for $Bi_2Sr_2CuO_6$ are determined in such a way that the calculated and measured frequencies for $O_z^\Gamma$ are very close, see table 4 and figure 4.

Moreover, we extract from the results in table 4 also that the other calculated Raman modes are improved by allowing CFs at these ions out of the CuO plane. In the case of $Bi_2Sr_2CuO_6$ it is remarkable that an infrared-active $A_{2u}$ mode is also softened by nearly 2 THz if the out-of-plane CFs are admitted in addition. As can be expected, in this mode the $O_z$ and the Bi ion are vibrating against each other, compare with figure 4. It should be noted that in calculations of the infrared- and Raman-active modes for $La_2CuO_4$ and $Nd_2CuO_4$ with CFs allowed in the Π model on $O_z$, La or Nd, respectively, these CF do only have a minor influence on the phonon frequencies.

In figures 5 and 6 the calculated phonon dispersion of $HgBa_2CuO_4$ and $Bi_2Sr_2CuO_6$ is displayed in the main symmetry direction $\Delta \sim (1,0,0)$, $\Sigma \sim (1,1,0)$ and $\Lambda \sim (0,0,1)$. In addition, an interpretation of the IXS-phonon spectra for $HgBa_2CuO_4$ [12, 54] and for $Bi_2Sr_2CuO_6$ [16] is added to the figures in the form of open squares and circles.

In the case of $HgBa_2CuO_4$ a minor deficit is visible in the form of one slightly unstable acoustic $\Lambda_3$ mode which is related to lattice vibrations propagating along the $c$ axis where the $O_z$ and Ba ions are vibrating in phase parallel to the CuO plane. This instability is already present in the RIM and most likely is a result of the more open structure of $HgBa_2CuO_4$ and thus of the growing importance of non-central forces.

The interpretation of the IXS spectra in [12, 54] and [16], respectively, are based on a Voigt fit. The positions of the peaks resulting from this fit are displayed in the IXS spectra shown in figure 7(a) for $HgBa_2CuO_4$ and in (b) for $Bi_2Sr_2CuO_6$ as open triangles. In addition, we have plotted in this figure the calculated frequencies of the $\Delta_1$ modes in the energy range considered, including the half-breathing mode, at the corresponding wavevectors (full triangles).

At first, one notices that for $HgBa_2CuO_4$ only one phonon peak has been fitted in the energy range shown in figure 7(a). On the other hand, we find in this range of energy a phonon spectrum which is much more complex comprising up to four

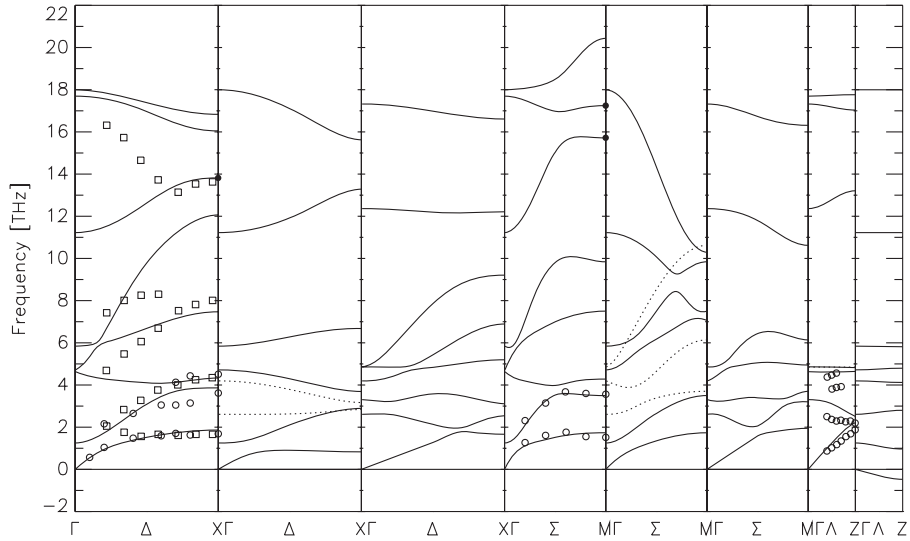


**Figure 5.** Calculated phonon dispersion of $HgBa_2CuO_4$ for model Π-3dim in the main symmetry directions $\Delta \sim (1, 0, 0)$, $\Sigma \sim (1, 1, 0)$ and $\Lambda \sim (0, 0, 1)$. The symbols ∘ and □ represent experimental results from [54] and [12], respectively. The circle ● marks two breathing modes at M and the half-breathing mode at X. The arrangement of the panels from left to right according to the different irreducible representations is as follows: $|\Delta_1|\Delta_2$ (· · · · · ·), $\Delta_4$ (——) $|\Delta_3|\Sigma_1|\Sigma_2$ (· · · · · ·), $\Sigma_4$ (——) $|\Sigma_3|\Lambda_1$ (——), $\Lambda_2$ (· · · · · ·) $|\Lambda_3|$. Imaginary frequencies are represented as negative numbers.

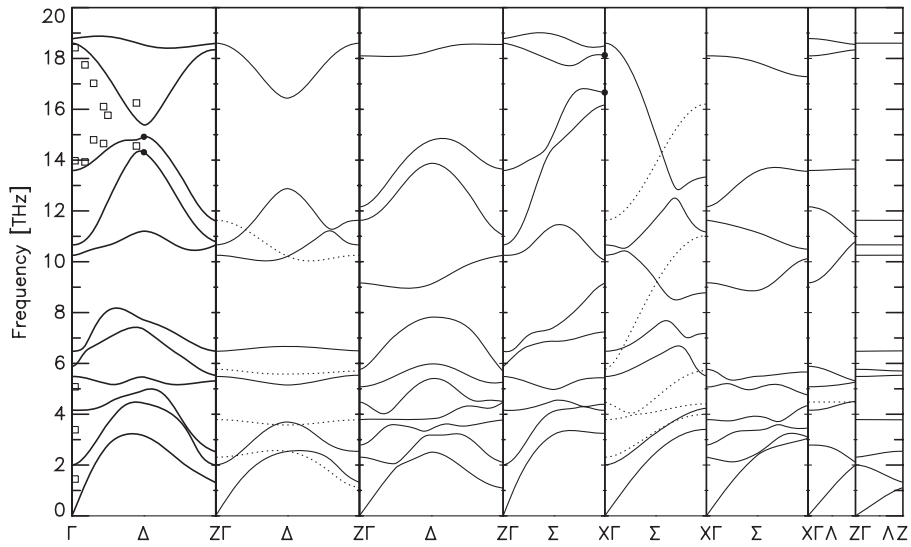


**Figure 6.** Calculated phonon dispersion of $Bi_2Sr_2CuO_6$ for model Π-3dim in the main symmetry directions $\Delta \sim (1, 0, 0)$, $\Sigma \sim (1, 1, 0)$ and $\Lambda \sim (0, 0, 1)$. The symbols □ represent experimental results from [16]. The circle ● marks the breathing modes at X and the half-breathing modes at $\Delta/2$. For the arrangement of the panels see figure 5.

$\Delta_1$ modes, see figure 5. In the fit for $Bi_2Sr_2CuO_6$ [16] only two phonon peaks have been fitted in the range of energy shown in figure 7(b), while according to our calculations in figure 6 there are up to five $\Delta_1$ modes in this range which can interact with each other and constitute a highly nontrivial anticrossing scenario. Quite generally, we can say that the IXS spectra reveal for small $\zeta$ values ($\mathbf{q} = (\zeta, 0, 0)$) in $HgBa_2CuO_4$ one and in $Bi_2Sr_2CuO_6$ two marked peaks. However, the strength of the peaks strongly decreases for larger $\zeta$ values such that at $\zeta \approx 0.5$ the peaks are very weak and an unique interpretation seems not possible. Moreover, the dips in the phonon dispersion curves as extracted from the interpretation of the IXS spectra at $\zeta = 0.36$ for $HgBa_2CuO_4$ [12] and at $\zeta = 0.25$ for $Bi_2Sr_2CuO_6$ [16] are not found in our calculations. However, as a result of the complex anticrossing scenario we obtain a pronounced dip at $\zeta = 0.5$ in $Bi_2Sr_2CuO_6$ and two half-breathing modes below the dip with somewhat smaller frequencies, see figure 6. The higher one has a displacement pattern as shown in figure 3(d) and in the lower one the apex oxygen and the oxygens in the ionic layer vibrate with opposite phases compared to figure 3(d). This also holds true for the X point, where two breathing modes occur, see figure 6. The higher one has the displacement pattern as shown in figure 3(d), and in the lower one the apex oxygen and the bismuth ion vibrate with opposite phases compared to figure 3(d).

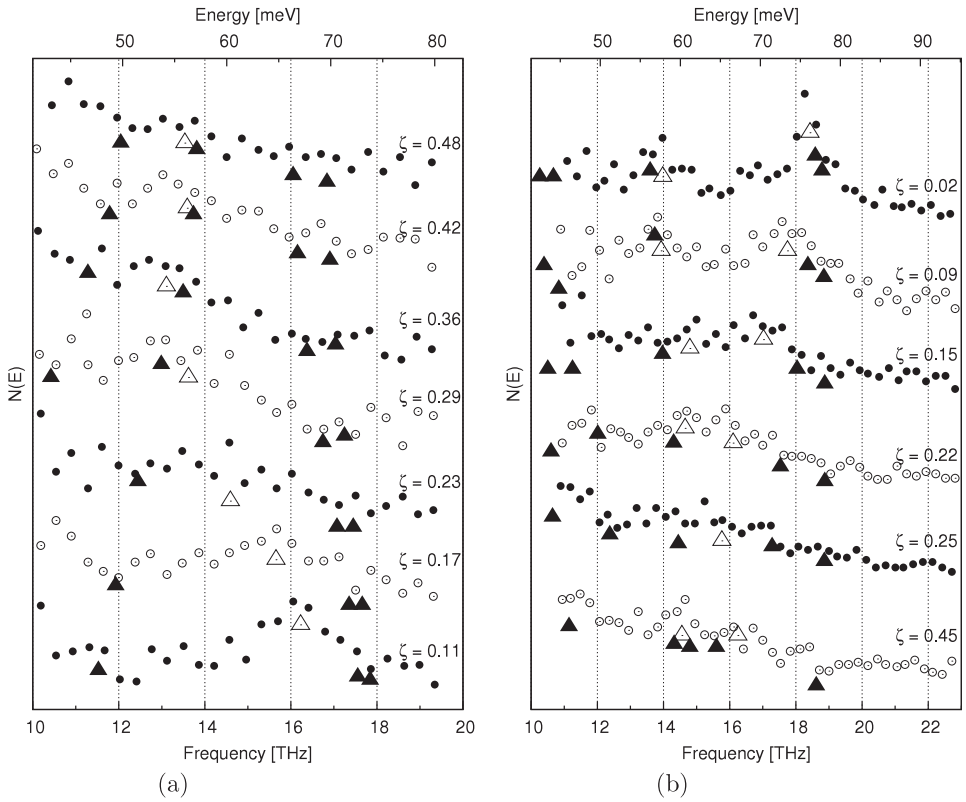


**Figure 7.** Reconstructed experimental x-ray spectra $N(E)$ of (a) $HgBa_2CuO_4$ for $\mathbf{q} = \frac{\pi}{a}(\zeta, 0, 0)$ [12] and (b) $Bi_2Sr_2CuO_6$ for $\mathbf{q} = \frac{2\pi}{a}(\zeta, 0, 0)$ [16] in arbitrary units, respectively. The experimental spectra for the different $\zeta$ are represented by the open and closed circles (○, ●). The according interpretations of the phonon frequencies fitted by a Voigt fit [12, 16] are represented by open triangles (△). Our calculated phonon frequencies are represented by closed triangles (▲).

In the case of $HgBa_2CuO_4$ we do not find a pronounced dip for the $\Delta_1$ modes in the relevant range of energy. We obtain as a result of four interacting $\Delta_1$ modes two branches with the highest frequencies showing a downward dispersion from Γ to X while the anomalous half-breathing mode is found at a lower energy and turns out to be the end point of the $\Delta_1$ branch with the third highest frequency. Similar to the case of $Bi_2Sr_2CuO_6$ we find in $HgBa_2CuO_4$ two breathing modes at the $M$ point. The lower one has a displacement pattern where the apex oxygen vibrates in the opposite direction as compared to the higher frequency breathing mode displayed in figure 3(c).

So, we guess from our calculations for $HgBa_2CuO_4$ and $Bi_2Sr_2CuO_6$ that the dip in the interpretation of the IXS spectra may be an artifact of the complex anticrossing behavior of several $\Delta_1$ modes in the frequency range under consideration. However, we admit concerning our results, that our microscopic model for the electronic polarizability applied to the calculation of the phonon dynamics of $HgBa_2CuO_4$ and $Bi_2Sr_2CuO_6$ is not fully *ab initio*.

The reliability of our calculated phonon dispersion may be judged from the conformance of our results with the phonon branches in $HgBa_2CuO_4$ at lower frequencies measured so far and displayed in figure 5 for the model Π-3dim.

The experimental and calculated results for the Raman- and infrared-active modes [56–60] are listed in table 4 for both compounds and a good agreement is found for the measured and calculated data in model Π-3dim. This fact, together with the good results in model Π-3dim for the dispersion, underlines the importance of the electronic polarization processes of certain ions in the ionic layers and in general of the physics of the third dimension perpendicular to the CuO plane.

The effect introduced by the CFs on the $O_z$, Hg and Bi ions outside of the CuO plane on the phonon dispersion by itself is demonstrated in figure 8 for both compounds by comparing the results of model Π-2dim (broken lines) with those of model Π-3dim (full lines). Only the branches are shown where large differences appear. The most significant renormalization of the dispersion emerges is for the modes with the highest frequencies.

Finally, in figure 9, the calculated phonon density of states (DOS) is shown for $HgBa_2CuO_4$ and $Bi_2Sr_2CuO_6$, respectively, and is compared with the experimental findings for both compounds. The theoretical results have been obtained with model Π-3dim. They compare quite well with the experimental results for both the width of the spectra and their peak structure. Of course,,the assignment of the peaks is difficult in detail because the experimental data are broadened.

A calculation of the partial phonon density of states, not shown in this work, demonstrates that the DOS in the lower-frequency range is dominated by Cu, Ba and Hg vibrations and by Cu, Bi and Sr vibrations, respectively. On the other hand, the high-frequency part of the spectrum is nearly exclusively governed by oxygen modes.

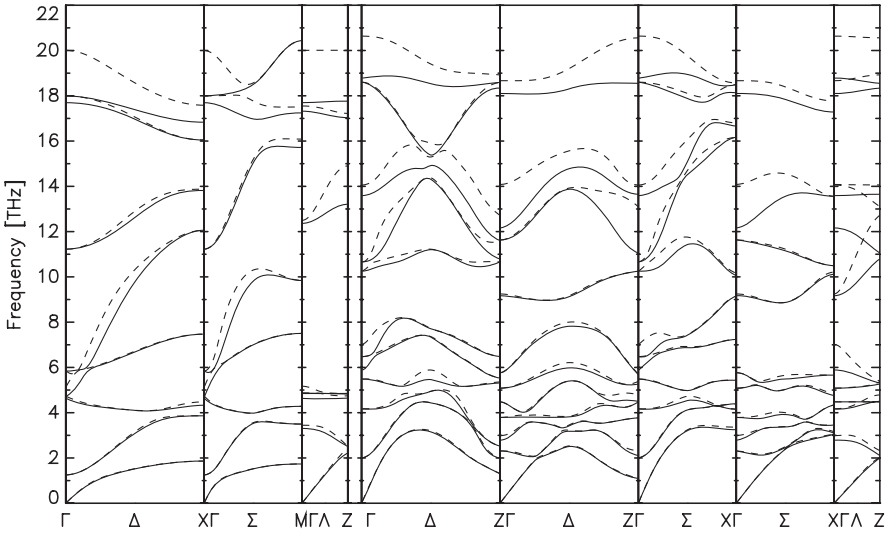


**Figure 8.** Comparison of model Π-2dim (- - - -) and model Π-3dim (——). The three leftmost panels belong to $HgBa_2CuO_4$ and the five rightmost panels belong to $Bi_2Sr_2CuO_6$. Only irreducible representations with a different phonon dispersion in model Π-2dim and model Π-3dim are shown. The arrangement of the panels from left to right according to the different irreducible representations is as follows: $|\Delta_1|\Sigma_1|\Lambda_1||\Delta_1|\Delta_3|\Sigma_1|\Sigma_3|\Lambda_1|$.

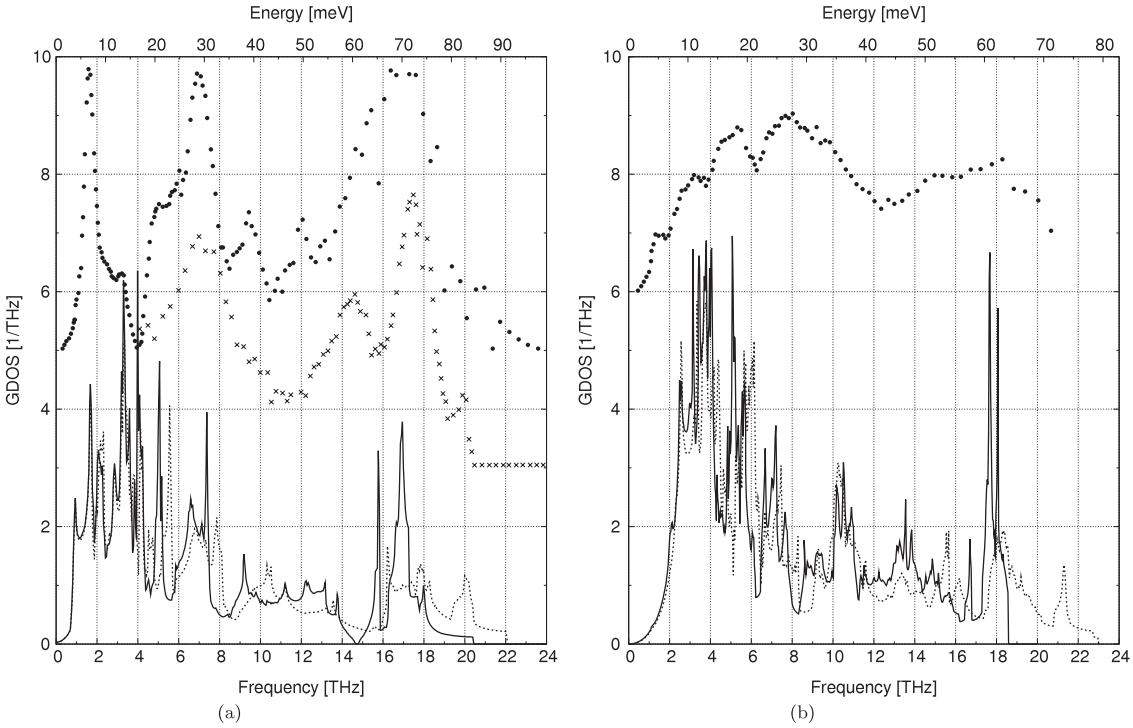


**Figure 9.** Calculated phonon density of states (DOS) for (a) $Hg_2BaCuO_4$ and (b) $Bi_2Sr_2CuO_6$ for model Π-3dim (——). For comparison, the DOS of the RIM is shown as a dotted line (· · · · · ·). The symbols × and • in (a) show the experimental data [61] at 30 and 300 K, respectively, while the symbols • in (b) represent the experimental data [62] at 300 K. All experimental data are in arbitrary units and shifted for better viewing.

From figures 9(a) and (b) the difference of the DOS in the model Π-3dim and the RIM generated by the electronic polarization processes can also be extracted. From the calculated results we find a significant decrease of the width of the spectra together with a characteristic redistribution of spectral weight, particularly in the high-frequency part. The latter is dominated by strongly coupling high-frequency oxygen vibrations living in this part of the spectra and suffering a corresponding softening compared to the RIM. The pronounced peaks which are generated by this softening also mean that there is considerable phase space for this strongly coupling modes.

## 4. Summary and conclusions

We have shown that for a reliable description of phonon dynamics and charge response in $HgBa_2CuO_4$ and $Bi_2Sr_2CuO_6$

a broad set of orbital degrees of freedom (Cu 3d, Cu 4s, O 2p) must be taken into account to model the electronic structure of the CuO plane. Moreover, for an ample representation of the real three-dimensional compounds electronic degrees of freedom beyond the strictly two-dimensional electronic structure must be considered.

We found that in the link between the CuO plane and the ionic layers of the cuprates electronic polarization processes of CF type are essential at certain ions. In $HgBa_2CuO_4$ $O_z$ 2p and Hg 6s CFs and in $Bi_2Sr_2CuO_6$ $O_z$ 2p and Bi 6p CFs, respectively, are significant processes. CFs on these ions are promoted by the short distance of the $O_z$–Hg and $O_z$–Bi bond. Allowance of CFs on these ions outside of the CuO plane (model Π-3dim) leads to a much better depiction of the phonon dispersion curves, the Raman-active and the infrared-active modes, in particular for those where the apex oxygen vibrates along its bond with the Hg or Bi ion, respectively.

As far as the electronic degrees of freedom in the CuO plane are concerned we have pointed out that, besides the localized Cu 3d state and the O 2p state, the more delocalized Cu 4s state is also needed in the charge response for an adequate representation of the large softening of the high-frequency oxygen bond-stretching modes and the strong coupling to the electrons. Such an effect also has been found in our previous calculations for $La_2CuO_4$ and $Nd_2CuO_4$. The strong nonlocal coupling and the related strong renormalization of these modes seems to be generic in the cuprates.

Altogether, our calculated results for model Π-3dim are partly in good agreement with the phonon dispersion measured so far in $HgBa_2CuO_4$ and $Bi_2Sr_2CuO_6$ and also with the Raman-active and infrared-active modes.

However, we have pointed out that an interpretation of the IXS measurements of $HgBa_2CuO_4$ and $Bi_2Sr_2CuO_6$ in the high-frequency part of the spectrum and the assignment of dips in the corresponding phonon dispersion curves cannot be supported by our calculations. This is because our investigations show that, in the frequency range under study, we have multiple interacting phonon modes of $\Delta_1$ symmetry (four in $HgBa_2CuO_4$ and five in $Bi_2Sr_2CuO_6$) which create a complex anticrossing scenario that possibly cannot be studied correctly within a fitting using just one or two modes.

Finally, we have calculated the DOS of both compounds in satisfactory agreement with experiment. We found a significant redistribution of spectral weight due to the electronic polarization processes in particular in the high-frequency part of the spectrum. This energy range is dominated by the strongly coupling oxygen modes signaling a considerable amount of phase space for strong electron–phonon coupling.

## References


[1] Lanzara A *et al* 2001 *Nature* **412** 510
[2] Cuk T *et al* 2005 *Phys. Status Solidi* b **242** 11
[3] Pintschovius L 2005 *Phys. Status Solidi* b **242** 30
[4] Gweon G H *et al* 2004 *Nature* **430** 187
[5] Zhou X J *et al* 2005 *Phys. Rev. Lett.* **95** 117001
[6] Reznik D *et al* 2006 *Nature* **440** 1170
[7] Lee J *et al* 2006 *Nature* **442** 546
[8] Guo-meng Z 2007 *Phys. Rev.* B **75** R140510
Guo-meng Z 2007 *Phys. Rev.* B **75** 214507
[9] Pintschovius L and Reichardt W 1998 *Neutron Scattering in Layered Copper-Oxide Superconductors* (*Physics and Chemistry of Materials with Low Dimensional Structures* vol 20) ed A Furrer (Dordrecht: Kluwer Academic)
[10] Pintschovius L and Braden M 1999 *Phys. Rev.* B **60** R15039
[11] Reichardt W 1996 *J. Low Temp. Phys.* **105** 807
[12] Uchiyama H *et al* 2004 *Phys. Rev. Lett.* **92** 197005
[13] Fukuda T *et al* 2005 *Phys. Rev.* B **71** R060501
[14] Pintschovius L *et al* 2006 *Phys. Rev.* B **74** 174514
[15] McQueeney R J *et al* 2001 *Phys. Rev. Lett.* **87** 077001
[16] Graf J *et al* 2008 *Phys. Rev. Lett.* **100** 227002
[17] d'Astuto M *et al* 2002 *Phys. Rev. Lett.* **88** 167002
[18] d'Astuto M *et al* 2003 *Int. J. Mod. Phys.* B **17** 484
[19] Braden M *et al* 2005 *Phys. Rev.* B **72** 184517
[20] Bauer T and Falter C 2008 *Phys. Rev.* B **77** 144503
[21] d'Astuto M *et al* 2008 *Phys. Rev.* B **78** R140511
[22] Falter C 2005 *Phys. Status Solidi* b **242** 78
[23] Falter C, Klenner M and Ludwig L 1993 *Phys. Rev.* B **47** 5390
[24] Falter C, Bauer T and Schnetgöke F 2006 *Phys. Rev.* B **73** 224502
[25] Falter C *et al* 1997 *Phys. Rev.* B **55** 3308
[26] Bauer T and Falter C 2009 *Phys. Rev.* B **80** 094525
[27] Alexandrov A S 1992 *Phys. Rev.* B **46** 2838
[28] Alexandrov A S 1996 *Phys. Rev.* B **53** 2863
[29] Hardy T M *et al* 2009 *Phys. Rev.* B **79** 212501
[30] Falter C *et al* 1999 *Phys. Rev.* B **60** 12051
[31] Falter C 1988 *Phys. Rep.* **164** 1
[32] Falter C, Klenner M and Hoffmann G A 1995 *Phys. Rev.* B **52** 3702
[33] Falter C and Schnetgöke F 2002 *Phys. Rev.* B **65** 054510
[34] Perdew J P and Zunger A 1981 *Phys. Rev.* B **23** 5048
[35] Krakauer H, Pickett W E and Cohen R E 1998 *J. Supercond.* **1** 11
[36] Savrasov S Y and Andersen O K 1996 *Phys. Rev. Lett.* **77** 4430
[37] Wang C Z, Yu R and Krakauer H 1999 *Phys. Rev.* B **59** 9278
[38] Bohnen K P, Heid R and Krauss M 2003 *Europhys. Lett.* **64** 104
[39] Giustino F, Cohen M L and Louie S G 2008 *Nature* **452** 975
[40] Catlow C R A, Islam M S and Zhang X 1998 *J. Phys.: Condens. Matter* **10** L49
[41] Islam M S *et al* 1988 *J. Phys. C: Solid State Phys.* **21** L109
[42] Zhang X and Catlow C R A 1991 *J. Mater. Chem.* **1** 233
[43] Longo J M and Raccah P M 1973 *J. Solid State Chem.* **6** 526
[44] Müller Buschbaum H and Wollschläger W 1975 *Z. Anorg. Allg. Chem.* **414** 76
[45] Wagner J L *et al* 1993 *Physica* C **210** 447
[46] Torardi C C *et al* 1988 *Phys. Rev.* B **38** 225
[47] Falter C and Schnetgöke F 2003 *J. Phys.: Condens. Matter* **15** 8495
[48] Falter C and Hoffmann G 2000 *Phys. Rev.* B **61** 14537
[49] Andersen O K *et al* 1995 *J. Phys. Chem. Solids* **56** 1573
[50] Pavarini E *et al* 2001 *Phys. Rev. Lett.* **87** 047003
[51] Vielsack G *et al* 1990 *Phys. Status Solidi* b **158** 249
[52] De Weert M J *et al* 1989 *Phys. Rev.* B **39** 4235
[53] Bauer T and Falter C 2009 *J. Phys.: Condens. Matter* **21** 395701
[54] d'Astuto M *et al* 2003 *J. Phys.: Condens. Matter* **15** 8827
[55] Falter C, Hoffman G A and Schnetgöke F 2002 *J. Phys.: Condens. Matter* **14** 3239
[56] Krantz M C *et al* 1994 *Phys. Rev.* B **55** 1165
[57] Osada M *et al* 1997 *Phys. Rev.* B **56** 2847
[58] Liu R *et al* 1992 *Phys. Rev.* B **45** 7392
[59] Singley J 2009 private communication
[60] Kovaleva N N *et al* 2004 *Phys. Rev.* B **69** 54511
[61] Renker B *et al* 1996 *J. Low Temp. Phys.* **105** 843
[62] Parshin P P 1996 *Phys. Solid State* **38** 919